

Implementation of Active Infrared NDT Techniques Using Long Square Heating Pulses

G. Pitarresi¹

Abstract: The present work describes the implementation of active IR Thermography techniques for the NDT of thick polymer and glass-fibre reinforced polymer (GRP) composite panels. A low cost Thermal NDT set-up is proposed, comprising a single-detector IR camera with low thermal resolution and low frame rate, and common low-power halogen lamps as external heat source devices. The use of halogen lamps in particular requires several seconds of switch-on time in order to deliver meaningful and effective heat quantities. The influence of such long heat deposition intervals is investigated on the possibility to implement Transient Thermography and Lock-In Thermography techniques. Regarding the Transient Thermography approach this is carried out as in traditional Pulsed Thermography, and the Thermal Contrast is in particular analyzed assessing the influence of the heat pulse duration and non-uniformity of heat deposition. Regarding the Lock-In approach a technique is adopted which modulates heat deposition into trains of square waves. A lock-in signal processing in the frequency domain is then performed to obtain Phase Contrast parameters.

Keywords: NDT, Infrared, Transient Thermography, Lock-In Thermography, Long Square Heating.

1 Introduction

The present work describes the implementation of active IR-NDT techniques by using low cost equipment to evaluate the extent of interlaminar damage on thick Fibre Reinforced Plastic (FRP) composite polymer panels for primary structural applications.

In the last years IR-NDT is receiving increasing attention for its potentials as a non-contact full field, fast technique for the health monitoring of polymer composite structures. This attention is mainly driven by the strong demand for developing

¹ Università degli Studi di Palermo - Dipartimento di Ingegneria Chimica, Gestionale, Informatica e Meccanica (DICGIM), Viale delle Scienze (Ed. 8), 90128 Palermo - giuseppe.pitarresi@unipa.it.

improved robust techniques, which could be in-situ implemented at low costs, deployable also in not carefully controlled environments (e.g. boatyards, building sites, etc...) and providing fast analyses over large surfaces. Some recent implementations of IR-NDT on various fields have been reviewed, providing a state of the art scenario on actual and potential industrial applications, e.g. see [Taillade, Quiertant, Benzarti, Aubagnac (2011)] for applications of FRP composites in the building sector, [Amenabar, Mendikute, López-Arraiza, Lizaranzu and Aurrekoetxea (2011)] for the wind energy sector, [Breitenstein, Warta, Langenkamp (2010)] for electronic devices, [Ptaszek, Cawley, Almond, Pickering (2012)] on the evaluation of thermal barriers, [Garnier, G; Pastor, M. L.; Eyma, F.; Lorrain, B. (2011)] and [Avdelidis, Almond, Dobbinson, Hawtin, Ibarra-Castanedo and Maldague (2004)] for aircraft maintenance, [Greene (2012)] and [Sheppard, Phillips and Cooper (2009)] for marine composite structures and marine fleets maintenance. It is in particular observed how IR-NDT techniques become a first option, together with Shearography, when it comes to evaluate shallow defects over large surfaces (for a comparison of these methods see [Taillade, Quiertant, Benzarti and Aubagnac (2011), Pickering and Almond (2010), Garnier, Pastor, Eyma and Lorrain (2011), Amenabar, Mendikute, López-Arraiza, Lizaranzu and Aurrekoetxea (2011)]).

IR Thermography techniques in particular are based on evaluating temporal temperature evolution after or during the deposition of a thermal/mechanical external stimulus: active thermography [Maldague (2003), Meola and Carlomagno (2004) and Ibarra-Castanedo, Genest, Avdelidis, Jen, Piau, Guilbert, Maldague and Bendada (2009)]. Sub-surface defects usually disturb the surface distribution of temperature through different mechanisms (heat conduction perturbation, heat sinks, local frictional effects, etc.). Enhanced defect signatures are then retrieved through different signal processing analyses which, together with the nature of the external perturbing stimulus, characterize the various proposed IR-NDT techniques. These can be classified in general as: Transient Thermography (TT) or Modulated Thermography (MT).

TT techniques consider the surface cooling kinetics following the heating event, which more often consists in a short heat pulse delivered through flash lamps. Pulsed Thermography (PT) in particular consists in studying the quantitative and qualitative correlation between defect features and suitable thermal contrast parameters. Pulsed Phase Thermography (PPT) considers phase-signal contrast parameters obtained by analyzing the temperature drop evolution in the frequency domain [Maldague and Marinetti (1996), Ibarra-Castanedo (2005)].

MT techniques consider the response in the frequency domain of the temperature acquired during the deposition of an opportunely modulated heat wave. A lock-in

correlation between the deployed heat and the structure temperature response is performed to obtain phase contrast defect signatures. Traditional Lock-In Thermography (LI) has considered pure sinusoidal heat waves [Busse, Wu and Karpen (1992), Wu and Busse (1998), Giorleo and Meola (2002), Choi, Kang, Park, Kim and Kim (2008), Montanini, R. (2010)], with a major disadvantage given by the need to perform various experiments at different sine wave frequencies in order to better probe the material at different depths. More recently a number of authors have proposed the adoption of frequency modulated external heat deployment in order to launch in only one go many different harmonics on the structure and retrieve the phase information from analyzing the frequency content of the acquired temperature, e.g. through Fourier analysis [Pitarresi (2010), Liu, Wang and Dai (2010), Breitenstein, Warta and Langenkamp (2010), Ghali and Mulaveesala (2011), Chatterjee, Tuli, Pickering and Almond (2011)]. One advantage of MT techniques consists in the use of low power cheaper lamps, since the heat energy is provided over a longer time. This advantage is though partly lost in terms of costs when further equipment is considered to control and modulate the heating signal.

In this study the PT approach and the LI approach are both opportunely implemented in order to use a low cost experimental set-up. This is achieved by the use of a low thermal resolution, low frame-rate, single-detector IR camera and by common commercial halogen lamps as external heating sources. No further electronic device is used to control the heat emitted by the halogen lamps, and all the signal post-processing is performed via common commercial software through customizable Matlab® routines. One particular aspect related with manually controlling the heating lamps is that only long heat pulses can be managed, of the order of few seconds at least.

In the implemented PT approach the influence of long step heating and the low sampling rate of the IR camera determine various situations where at the end of the heating phase the defected site is already warmer than equally heated sound zones, in particular for shallower defects. This aspect, together with the non-uniformity of the deposited heat, is considered for the identification of suitable reference sound zones and the definition of thermal contrast parameters.

Regarding the LI approach the work considers the implementation of a train of square waves which are generated by periodically shattering the optical path between the lamp and the sample. This also allows the modulation into a single signal of a wider range of frequency components. A customized lock-in algorithm is then implemented which is able to selectively filter and correlate the measured temperature harmonics at various frequencies, and obtains phasegrams with enhanced defect signatures.

Both proposed approaches, the transient and the modulated, are implemented upon

a thick Glass-Fiber Reinforced Plastic (GRP) panel containing artificial defects which simulate interlaminar delaminations at surface depths ranging from 3 to 9 mm. A polycarbonate plate with machined blind back holes of different diameter is also considered in the assessment of the pulse-modulated lock-in approach.

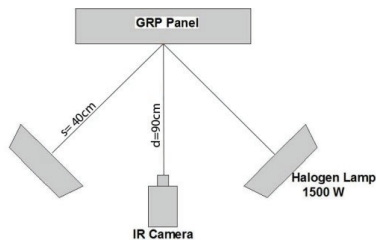
2 Description of the experimental set-up

A reflection scheme is adopted with a GRP defected panel facing the halogen lamps and the IR camera as shown in Fig. 1a,b. A personal computer is used to remotely control the IR camera acquisition, while all the signal processing required to retrieve and analyze the thermal and phase contrast was performed off-line by means of the software Matlab®.

2.1 Preparation of samples

The first analysed sample is a GRP panel manufactured by hand lay-up, with a symmetric cross-ply lay-up $[(0,90)_7]_s$, areal dimensions of $290 \times 290 \text{ mm}^2$ and thickness of 12 mm. The dry reinforcement was a unidirectional fabric with 400 g/m^2 areal weight. A polyester resin was used to impregnate the fabric, with curing achieved at room temperature under light pressure to obtain a final 35% fibre-volume fraction. A rough opaque surface finish was also obtained by laying a peel-ply sheet between the panel and the mould plates.

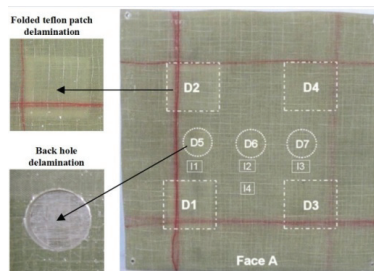
Seven defected zones were artificially introduced in the panel, all simulating delaminations (see Fig. 1c and Tab. 1). Four of these (referred to as D1, D2, D3 and D4) consisted in embedded Teflon pockets introduced during the panel fabrication. The Teflon sheet used was 0.04 mm thick. Rectangular patches of Teflon sheets were cut with dimensions $60 \times 100 \text{ mm}^2$. These were then two-folded and sealed on the border in order to avoid resin to flow inside. The final folded patches were then $60 \times 50 \text{ mm}^2$ wide. This Teflon pocketed patches were used to ensure a thin air layer to be trapped in the defect location, since Teflon material does not fully succeed in simulating the change in thermal diffusivity typical of a natural delamination. Three further defects (named D5, D6, D7) were introduced by drilling circular blind back holes of 30 mm in diameter. This artificial way to simulate a delamination is a common practice in the literature [Giorleo and Meola (2002)], to simulate the low heat diffusion characterizing a delaminated site. It is observed though that delaminations from impact, fatigue or other structural failure events, usually leave the flanks of the crack in contact, so that heat diffusion, and hence the thermal contrast typical of real cracks, should be expected somewhat less than that produced with drilled back holes [Polimeno and Almond (2009)]. The dimensions and depths from the surfaces of all defected zones are summarized in table



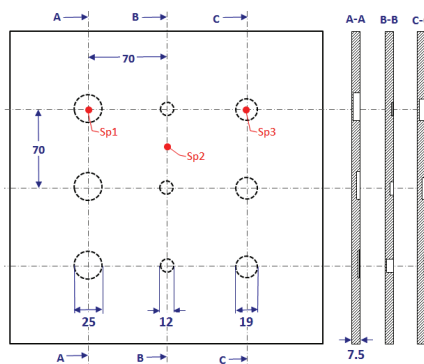
(a)



(b)



(c)



(d)

Figure 1: a) experimental reflexion scheme; b) photo of the experimental set-up; c) GRP panel with defects; d) Polycarbonate panel with back drilled blind holes of depth 1.5, 4.5 and 6 mm.

1. A second polycarbonate plate is also considered during the experimental implementation of the pulse-modulated lock-in technique. The sample has a thickness of 7.5 mm and an array of 9 back drilled blind holes of dimensions and depth as schematically shown in fig. 1d.

Table 1: Details of delamination defects within the GRP sample.

	Folded Teflon patch		Blind back hole
dimensions	60x50 mm ²		Ø 30 mm
Depth [fraction of panel thickness/mm]			
D1 –D2	1/4	D5	1/4
D3 –D4	1/2	D6	1/2
		D7	3/3

2.2 IR camera and heat source equipment

The IR camera employed is a low cost single detector infrared scanner: Varioscanner 3022 by Jenoptik GmbH, with a thermoelectrically cooled MCT detector operating in the spectral range 3-5 μm , and having a NETD resolution of 0.12 K. Frame resolution is 360×240 pixels, acquired by raster scanning, with full frame rate slightly less than 1 Hz. The camera is remotely operated via a PC by means of the IRBIS[®] V3.0 software (further details on the features of this IR scanner can be found in [Pitarresi, D'Acquisto and Siddiolo (2008)]). The saved thermogram sequences have successively been imported in Matlab[®] as 8 bit grayscale bitmaps for further post-processing.

Two commercial 1.5 kW halogen lamps have been used as external heat devices. The lamps have been manually operated with no automatic modulation of the power supply and no accurate control of the switch on/off triggering time and heating interval. A polystyrene panel was in particular used to cover the lamps at the end of the heating interval. In the PT analysis this helped to make sure that no spurious heat could still reach the panel after switch off due the residual warmth of the lamp. In the LI analysis the cover was manually placed to periodically shutter the optical path from the lamp to the panel, in order to modulate the deposited heat as a train of square waves.

3 Pulsed Thermography analysis

The vast majority of studies implementing PT uses flash lamps able to deliver consistent heat quantities in few milliseconds [Maldague (2003), Ibarra-Castanedo,

Genest, Avdelidis, Jen, Piau, Guilbert, Maldague and Bendada (2009)]. Furthermore the very early cooling transitory stage after the heat pulse deposition is usually sampled by high speed FPA IR cameras. This combination of equipment performances allows for some advantages:

1. it is possible to use the early cooling stage for a theoretical reconstruction of the reference cooling properties of the sound material, e.g. through techniques such as the TSR [Shepard, Hou, Lhota and Golden (2007)] and the DAC [Ibarra-Castanedo, Benitez, Maldague and Bendada (2007), Benitez, Loaiza, Caicedo, Ibarra-Castanedo, Bendada and Maldague (2009)], avoiding the problems related with identifying a proper sound area;
2. a detailed early sampling may allow the use of early detection parameters (e.g. time of emerging thermal contrast) which can better correlate with defect depth retrieval (see for instance [Balageas (2010), Krapez and Balageas (1995), Martin, Gyekenyesi and Shepard (2003)]);
3. a short heat pulse can be modeled as a Dirac discontinuity and analytical solutions may be used to correlate the material heat diffusion length with defect depth and time at maximum thermal contrast [Maldague (2003), Krapez and Balageas (1995)].

Although such higher performance equipment for PT implementation has become more and more routinely available, it still represent a significant cost, and sometimes to gain only limited improvements in quantitative analysis over qualitative. This is particularly true with GRP polymer composites, for which thermal conduction kinetics are very slow and structural thicknesses can be consistent, with the need to deploy higher heat quantities to probe at proper higher depths.

The use of low power heating in TT techniques is less widespread due to the need to use long heating times (Square Pulse Thermography) [Dumoulin, Ibarra-Castanedo, Quiertant, Taillade, Bendada and Maldague (2010), Arndt (2010)], which enhance the difficulties in modeling all heat conduction phenomena and develop quantitative inverse procedures for defect characterization.

In the following subsections definitions of thermal contrast are recalled and the influence of long heating pulses and low sampling rates are analyzed for retrieval of quantitative information on defects features.

3.1 Thermal Contrast analysis with long square heating

In this work two definitions of thermal contrast are used in particular: Standard Contrast (C_s) and Normalised Contrast (C_n), both described in [Maldague (2003)],

and defined by:

$$C_s(t) = \frac{T_d(t) - T_d(t_o)}{T_s(t) - T_s(t_o)} \quad (1)$$

$$C_n(t) = \frac{T_d(t)}{T_d(t_m)} - \frac{T_s(t)}{T_s(t_m)} \quad (2)$$

where subscripts d stay for defected zone and s for sound zone, t is the time variable, t_o is the temperature before launching the heat pulse, and t_m is the first temperature measured after the lamps switch off, i.e. the first useful thermogram sampled in the cooling transitory. C_s and C_n are plotted vs. time as shown in Fig. 3,4, in which the origin is fixed at the t_m time. From these plots two parameters are in particular chosen for their potential ability to correlate with defects depth and size: the maximum contrast C_{max} , and the time of its occurrence, t_{max} .

In order to evaluate the curve of thermal contrast and the related parameters, three main difficulties have been identified, mainly related with the use of low performance equipment:

1. the IR camera low frame rate does not allow for an adequate sampling of the early cooling transitory, and the identification of a suitable sound area is required for evaluating $T_s(t)$;
2. it is not possible to control heating durations smaller than a few seconds, which, for shallower defects in particular, may induce an early accumulation of heat upon the defect already at or before t_m (i.e. there is a visible thermal contrast on the first acquired thermogram of the cooling transitory). In the following this situation will be addressed as *early contrast*;
3. usually the heat front deposited on the structure surface is not uniform. In this case a proper sound area for the calculation of thermal contrast in a given defect is the one that has received the same amount of heat then the defect being evaluated.

A procedure called Source Distribution Image (SDI), recently suggested by [Susa, Maldague and Boras (2010)] is able to deal with this last issue. This is based on the analysis of isotherm contours, taken soon after the heat pulse delivery. Once the defect location is identified, e.g. by a qualitative evaluation of later thermograms, the corresponding proper sound area is chosen on a sound location located on the same isotherm contour or at least one of the same order. The SDI procedure may though not be directly applicable in the above mentioned case ii (i.e. in presence of a pre-accumulated heat on the defected zone, i.e. early contrast).

A wrong choice of the reference sound zone for thermal contrast evaluation usually produces some well identifiable anomalies in the thermal contrast curves. In the following subsections some of these anomalies are identified and commented, providing helpful hints for the most proper choice of reference sound zones.

3.1.1 Factors potentially affecting the Standard Contrast C_s

It is usually plausible to assume that $T_d(t_o) = T_s(t_o)$, i.e. the initial temperature does not show any peculiar non-uniform pattern (uniform initial temperature). In this case C_s will initially grow starting always from unity. It will reach a maximum and then decrease but remaining above unity (which will be the asymptotic value to reach at restored equilibrium). In this scenario the following situations may arise:

1. $T_d(t_m) > T_s(t_m)$ and $C_s(0) > 1$. If the sound zone has received the same amount of heat than the defected zone, this first condition occurs when the defected zone has overheated (early contrast) during the pulse deposition;
2. $T_d(t_m) = T_s(t_m)$ and $C_s(0) = 1$. If the chosen sound zone has received the same amount of heat than the defected zone (e.g. the SDI procedure is applied), then the curve of the Contrast is correct. If the defect zone has developed an early contrast, the attempt to choose a sound zone verifying condition 2 will result in a sound zone that has received a higher heat quantity than the defected zone. Usually this results in an underestimation of the value of C_{smax} and sometimes to C_s eventually decreasing under unity. This is mainly due to the slower cooling of the sound zone;
3. $T_d(t_m) < T_s(t_m)$ and $C_s(0) < 1$. In this case the sound zone has always received a higher heat quantity than the defected zone, and hence a plot of a C_s curve starting from values smaller than 1 will always indicate a bad choice of the sound zone.

3.1.2 Factors potentially affecting the Normalised Contrast C_n

By definition the normalised contrast C_n (eq. 2) always starts from zero. If the sound zone is chosen correctly, then C_n will grow up from zero to reach a maximum at the time t_{cnmax} , and eventually decreases back to zero asymptotically. Two anomalies can usually arise from a non-ideal choice of the sound zone: the later occurring of negative values long after the heat delivery, and an initial marked steep gradient in the growth of C_n .

It is useful to consider the first derivative of C_n written as:

$$\frac{dC_n}{dt} = \left[\frac{1}{T_d(t_m)} \frac{dT_d}{dt} \right] - \left[\frac{1}{T_s(t_m)} \frac{dT_s}{dt} \right] \quad (3)$$

In the case of $T_d(t_m) = T_s(t_m)$ (e.g. no early contrast, or late initial sampling), there will be an initial time window during which the heat front has not reached the sub-surface resistive site yet, and $dT_s/dt = dT_d/dt$. The sampling in this window will give a zero value of the derivative in eq. 3. As the heat reaches the defective site and a thermal contrast starts to grow, the drop of T_d will slow down, and $dT_s/dt < dT_d/dt < 0$, so determining a positive value of the derivative given by eq. 3. In general C_n should then present a gradual growth from a horizontal tangent at the plot origin. Two circumstances can cause a deviation from this expected behavior:

1. $T_d(t_m) > T_s(t_m)$ and the sound zone has received the same heat as the defected zone. This situation can arise due to early contrast of the defected zone or a late start of sampling in the cooling transitory, when the thermal contrast has already started to build up. In both cases it will be $dT_s(t_m)/dt < dT_d(t_m)/dt < 0$ and C_n will have an initial positive slope.
2. $T_d(t_m) = T_s(t_m)$ but the defected zone experiences an early contrast. For this situation to arise the sound zone must be chosen in a zone which has received more heat than the defected zone. As a consequence T_s will keep unusual high values and lower cooling gradients which may determine anomalies such as initial negative gradients of C_n and values of C_n below zero at the initial or final parts of the C_n plot.

In general a poor choice of a reference sound zone, e.g. which has received a different amount of heat than the defected zone, may have a marked influence on values of thermal contrast, including C_{max} , regardless of the definition of thermal contrast used, normalized or standard. Regarding t_{max} its sensitivity to the choice of the sound zone is in general less marked.

It is possible to demonstrate that t_{max} from C_n and C_s is slightly different. In fact equating the first derivative of eq (1) to zero yields:

$$\frac{dC_s(t)}{dt} = 0 \rightarrow \frac{dT_d(t_{max})}{dt} = \frac{dT_s(t_{max})}{dt} C_s(t_{max}) < \frac{dT_s(t_{max})}{dt} \quad (4)$$

The less than sign in eq. (4) is justified by observing that $C_{s,max} > 1$, while in general dT/dt is always negative (cooling temperatures). Computing the derivative of eq. (2) and equating to zero yields:

$$\frac{dC_n(t)}{dt} = 0 \rightarrow \frac{dT_d(t_{max})}{dt} = \frac{dT_s(t_{max})}{dt} \frac{T_d(t_m)}{T_s(t_m)} = \frac{dT_s(t_{max})}{dt} \quad (5)$$

Equation (5) shows that for C_n the maximum contrast is reached when the slope of T_d equates the slope of T_s . From Equation (4) it is found that the maximum contrast

is achieved when the degrading slope of T_d is steeper than that of T_s , by a factor equal to C_{s_max} , and this condition occurs at longer times. Hence it is possible to conclude that $t_{max_Cs} > t_{max_Cn}$.

3.2 Experimental evaluation and discussion of results

Figures 2-4 show some results from the experimental implementation of the PT approach. The scheme in Fig. 1a evidences the mutual position of sample, IR camera and halogen lamps. All processed results in Fig. 2-4 were relative to a heat delivery time of 40 seconds. Figure 2 shows a thermogram contour map acquired after 20 seconds from the lamps switch off. With the exception of defect D7, all other defects are visible through a local disturbance of isotherms and a thermal contrast with the surrounding zones.

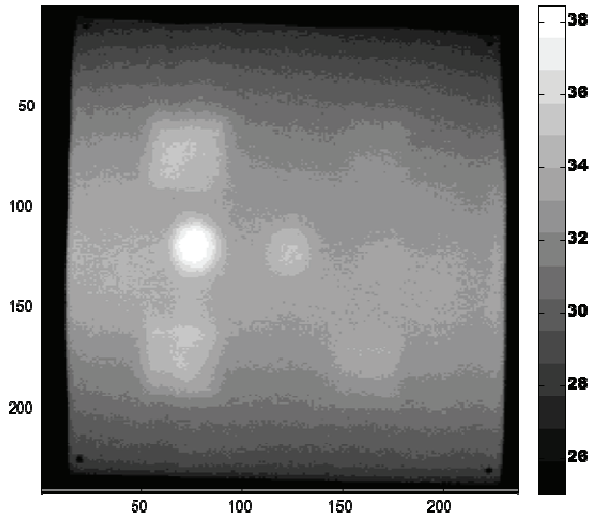


Figure 2: Contour Map of thermogram acquired 20 sec from the start of cooling transitory.

Figure 2 clearly evidences also a non-uniformity of heat deposition on the analysed panel. As evidenced before, the choice of proper sound zones may be greatly affected by such non-uniformity. Defect D3 in particular, an embedded Teflon pocket at 6 mm depth from the surface, did not generate early contrast during the external heat delivery. This was then chosen to evaluate the thermal contrast curves. Figures 3a,b show plots of C_n e C_s for this defect. For each of the two thermal contrast definitions four curves are reported, each obtained with a different sound area, whose position is indicated in Fig. 1c. Curves tagged as SDI are derived with a sound

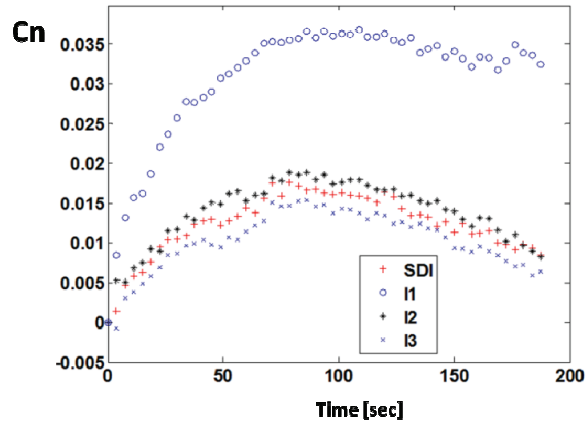
zone positioned after implementing the Source Digital Image technique, to guarantee the same heat input of the D3 zone. The SDI technique was implemented on the Matlab® contour plot of the first useful thermogram acquired after the lamps switch off. In implementing the SDI technique it is evidenced that while defects D1, D2 and D5 were well visible at lamps switch off after 40 sec (early contrast), all other defects did develop a visible contrast only after switch off.

Differences among the curves in Fig. 3a,b clearly evidence a marked influence of the choice of the sound zone. In the case of C_n , for instance use of sound zone II produced a more than double value of C_{max} compared to other sound regions, while the t_{max} did not show a similar fluctuation. In the case of C_s again the contrast value is much affected by the sound zone, with some curves staying well below or starting above the initial unity value, with the exception of the SDI curve. It is interesting to observe that the t_{max} parameter for C_s is again less influenced by the choice of sound zone, and values are slightly higher than those from C_n curves, confirming the theoretical considerations based on eqs. (4,5).

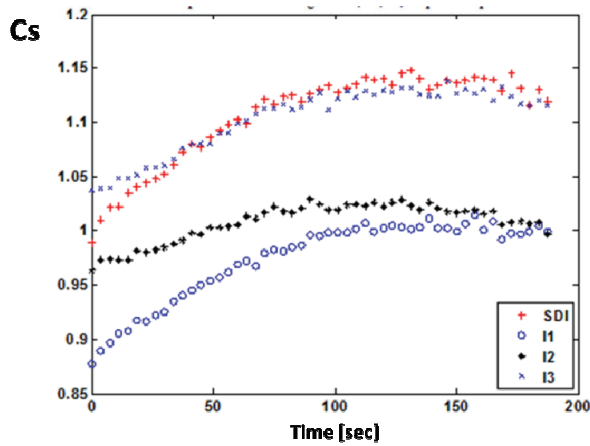
In general the SDI technique has been effective in reducing some anomalies in the contrast curves as commented in section 3.1, and this treatment becomes essential if the C_{max} value is to be used to correlate defects features. This is evident in Fig. 4, where the C_n curves, computed with SDI compliant sound zones, and referred to defects D3 (embedded teflon) and D6 (blind back hole), are compared. The two defects have similar sizes and equal depth (6 mm). The t_{max} is similar for both defects but the C_{max} is much higher for D6. This is explained by the higher thermal resistance that a blind hole is able to introduce than a Teflon patch. In fact Teflon material and polyester based GRPs do not have a mismatch in thermal diffusivity and effusivity as severe as the GRP material with air [Ibarra-Castanedo (2005)]. Very few works in the literature have investigated the ability of artificial defects (as typically employed for IR NDT studies) to simulate the behavior of natural delaminations. It is commented here that natural delaminations usually have trapped air but also zones where the crack flanks are in contact, in particular near the crack tip borders. This induces to believe that the typical thermal resistance of a natural delamination is probably smaller than a blind hole, and likely closer to the condition of a Teflon pocket as employed in this work.

Some further conclusions are finally summarized as follows:

Heat deposition times as low as 10 seconds have been applied but did not allow to get rid of early contrast on defects D1, D2 e D5 (all at 3 mm depth). The attempt to apply heat deposition at shorter times was not successful as this reduced too much the heat delivered and very poor thermal contrast was obtained. A higher resolution and faster frame rate IR camera would probably be needed to deal with such shorter heat pulses. The early contrast problem did not allow the reliable application of the



(a)



(b)

Figure 3: a) Curves of Normalised Contrast at varying reference sound area; b) Curves of Standard Contrast at varying reference sound area.

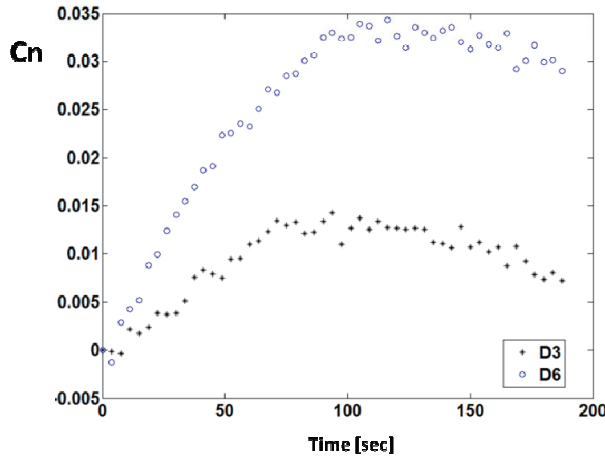


Figure 4: Comparison of Normalised Contrast for defects D3 and D6 (Teflon patch vs blind back hole).

SDI technique and evaluation of comparable t_{max} and C_{max} parameters. On the contrary defects were very well visible, and their qualitative detection was straight forward.

Defects at 6 mm depth (D3 and D6) generally did develop a satisfactory thermal contrast only with heating times higher than 20 sec. Defects at 9 mm depth (i.e. D4 and D7) did not develop a satisfactory thermal contrast with heat deposition times as high as 80 sec.

In general, for defects at equal depth, the C_{max} parameter is more sensitive to the choice of the sound zone, to the heat source power, to the heat deposition time interval and to the type of artificial defect, while t_{max} is more sensitive to the total delivered heat quantity, and less sensitive to the other experimental variables.

4 Pulse-Modulated Lock-In Thermography analysis

Although Modulated Lock-In Thermography is a well established technique for defect signature enhancement through phase contrast evaluation, its implementation is perhaps not as much widespread as TT Techniques. One reason for this is the common practice of modulating the heat delivery into a pure sinusoidal wave or some carefully controlled signal shapes, which requires some additional electronic devices and a somewhat more complex experimental set-up and signal processing. The analysis in the previous section has evidenced the slow evolution of thermal phenomena in GRP structures, with the general need of rather long heat delivery

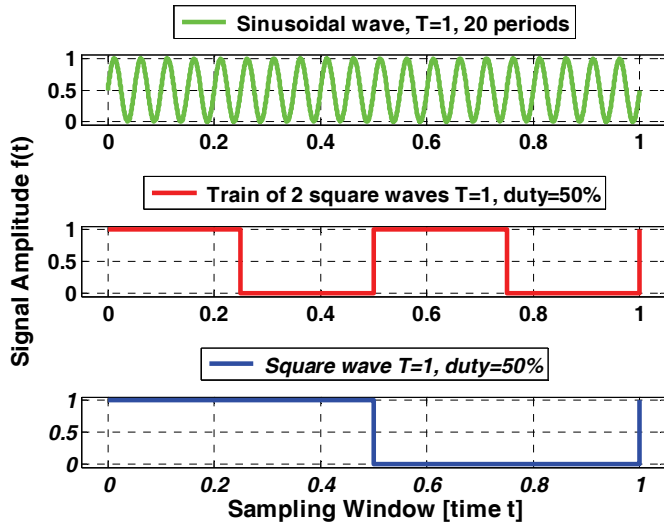
intervals to activate the desired thermal response. These conditions have allowed the possibility to manually modulate the heat from one halogen lamp, in order to contemporarily launch a number of harmonics at different frequencies. A mean to implement this heating strategy, at no further costs, is by simply shuttering periodically the path between the lamp and the panel in order to modulate the delivered heat into a train of square waves. The sample temperature is acquired during heat deposition, and is analyzed in the frequency domain, to filter out the phase information. A Matlab[®] algorithm is in particular implemented that is able to filter harmonics at various frequencies in order to retrieve the phase information [Pitarresi, D'Acquisto, Siddiolo (2008), Pitarresi (2010), Pitarresi (2012)]. The following subsections will present some more details of the analysis performed.

4.1 Modulation of the heat source

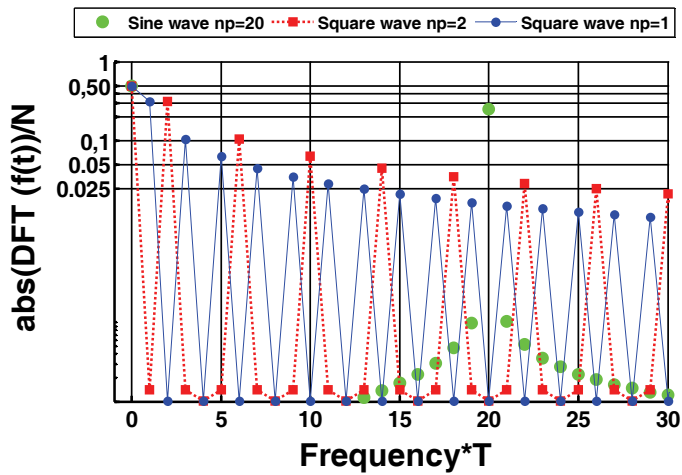
In order to understand the mechanism of multiple harmonics deployment behind the modulation of the heat wave launched onto the sample, a Discrete Fourier Transform (DFT) analysis of various periodic signals is proposed in Fig. 5. The computation, performed in Matlab[®] considers a time window of duration T (normalized to $T=1$ for a more general discussion), in which a pure sinusoidal signal is contained with 20 periods, a square wave of equal amplitude with 2 periods, and a square wave of equal amplitude with one period. The power spectrum revealing the frequency content of these signals is reported in Fig. 5b and obtained by a discrete fft analysis (with N indicating the total number of sampled points). It is observed that the sine wave carries most of the power at a single frequency, while the square waves have several harmonics at lower frequencies which contain a portion of the total carried power.

The low frequency harmonics content of square waves increases with decreasing the square wave principal carrier frequency. The ability of a sinusoidal heat wave to probe the inner state of the material is governed by the wave frequency [Giorleo and Meola (2002), Choi, Kang, Park, Kim, Kim (2008)]. Generally lower frequencies can probe at deeper depths. So the opportunity to distribute the delivered heat onto a wider range of low frequency harmonics is related with the possibility to use each frequency to probe at different depths [Pitarresi (2010), Ghali and Mulaveesala (2011)].

One further feature that is implemented in this work is the modulation of trains of square waves with different duty cycles, dc , with this parameter describing the ratio of non-zero vs zero signal within one period. So a square wave with $dc=50\%$ has a null value for the 50% of its period. Fig. 6 analyses the frequency content of three square waves with different dc , evidencing the influence of the different modulation onto the low frequency harmonic content.



(a)



(b)

Figure 5: a) Analysed periodic waves; b) Power Spectrum with frequency content from the Discrete Fourier Transform, normalised by the total number of samples N .

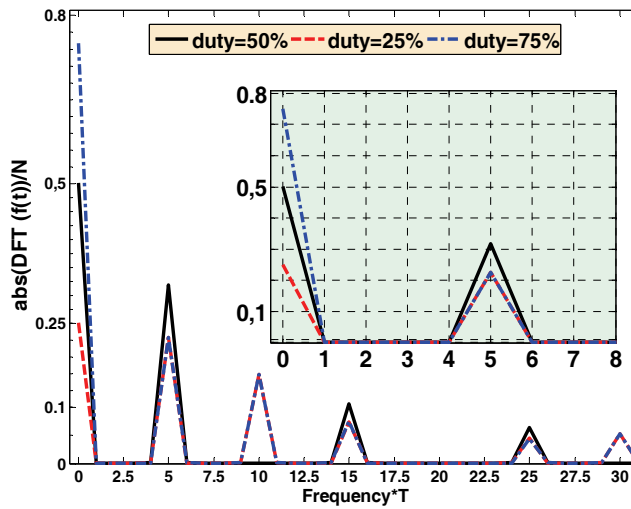
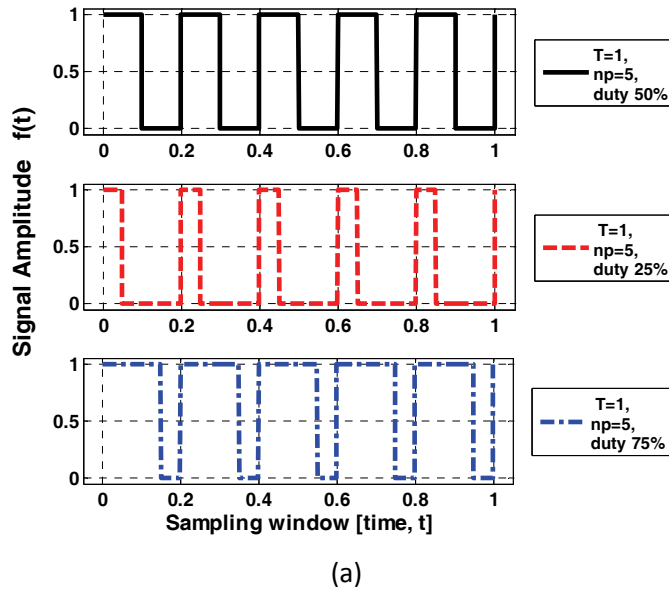


Figure 6: a) Trains of square waves with varying duty cycle; b) Power spectrum in the low frequency domain of the train waves.

4.2 Lock-In correlation scheme

The sampled thermographic signal is post-processed by means of a lock-in correlation algorithm that is schematically outlined in Fig. 7. The acquired signal S is in particular mixed with a pure sinusoidal reference wave F and its in-quadrature shifted counterpart G . The result of the subsequent steps is the extraction from S of the amplitude and phase content at the same frequency as the reference signal F . This is in particular achieved by implementing a low pass filter on the mixed $S \cdot F$ and $S \cdot G$ signals. Hence for each reference frequency value an iteration of the algorithm can be run and the corresponding phase shift between S and F retrieved.

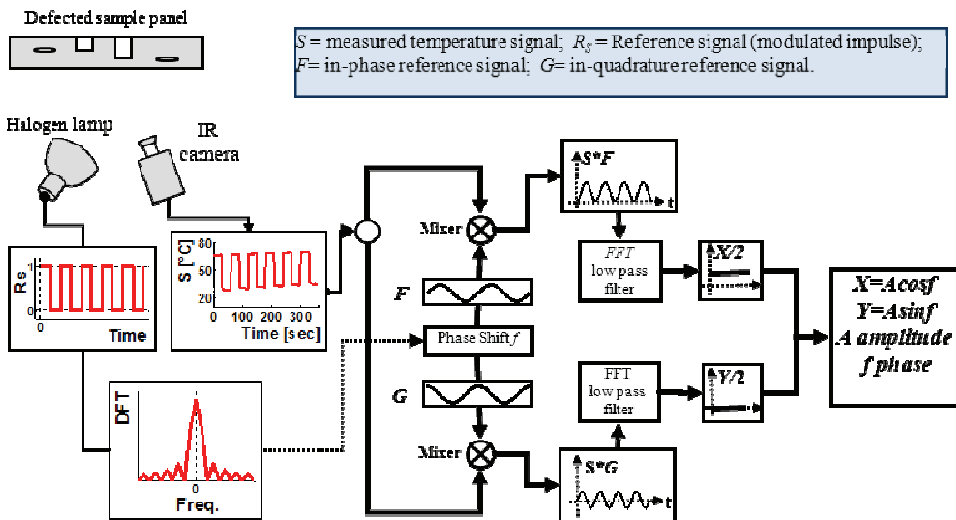


Figure 7: Scheme of the Lock-In correlation.

One advantage of the proposed lock-in algorithm is the possibility to obtain the phase shift information for various frequencies. By computing this analysis on the signal coming from each pixel of the acquired sequence of thermograms, it is then possible to obtain a phasegrams for each value of frequency set in the lock—in algorithm. One further advantage of this approach, as compared with the traditional *Four-Point Correlation Method* used in literature (see for instance [Liu, Wang and Dai (2010)]), is the intrinsic capacity of the algorithm to filter out noise (in particular high frequency noise) from the measured signal, through the implementation of low-pass filters.

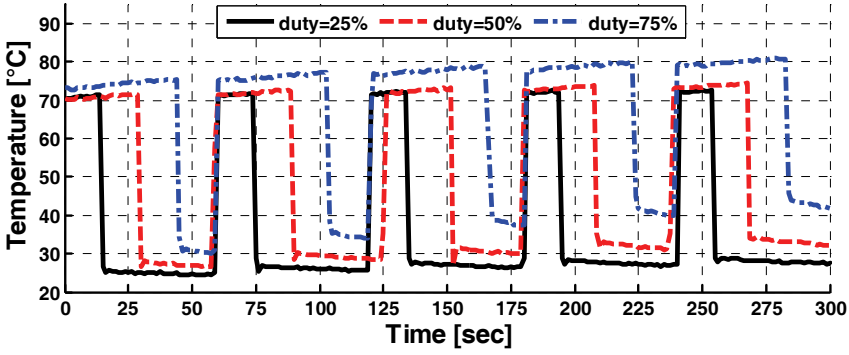
4.3 Experimental implementation and discussion of results

Three acquisitions have been taken from the GRP sample, with only one lamp operated from a distance of about 1.25 m from the panel, laterally positioned as in fig. 1a. Each acquisition lasted 5 minutes during which the train of square waves was modulated such to deliver 5 periods of 60 sec each. The three tests differed only for the duty cycle modulation, with values of dc respectively of 25%, 50%, 75%.

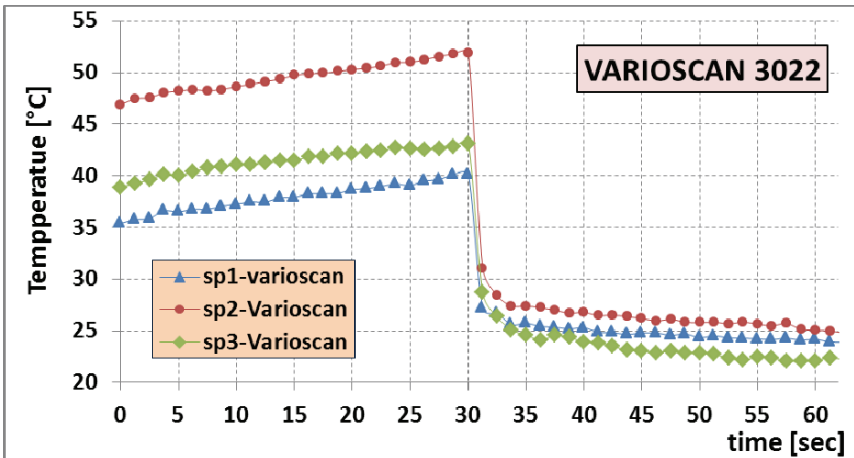
The lock-in analysis performed with different frequency values found that the best phase contrast was obtained with very low frequencies (lower than the carrier frequency used to generate the train waves). Figure 8 shows the three phasegrams (one for each applied duty cycle) obtained with a lock-in frequency of 3.3 mHz. It is interesting to observe how this value is smaller (one fifth) of the main carrier frequency of the applied train wave which is 16.7 mHz. In fact by exploiting the ability of the implemented lock-in algorithm, it has been possible to observe that while correlation at the main carrier frequency did result in poor phase contrast, the optimal value was achieved at 3.3 mHz.

Figure 8a shows the temperature-time profiles referred to a pixel of the analysed area, while fig. 9 shows the obtained phase maps. The phasegram referred to the train wave at $dc=25\%$ produced the higher phase contrasts on all seven defected zones. It is meaningful to observe that the deepest defects D7 and D4 are well visible in all three maps in Fig. 8. So despite the non-conventional implementation of the transient and modulated thermography techniques proposed in this work, it is found that Modulated Thermography is still able to probe deeper. It is interesting to observe also that with duty cycles of 50% and 75% a slight non-uniform phase shift is present between the sound zones in the central part and outer part of the panel. Such non-uniformity is probably introduced by slower heat dissipation in the central part of the panel than the outer zones. Due to this non-uniformity, a calculation of phase contrast would be influenced by the choice of the sound zone in a way similar to what discussed in section 3.

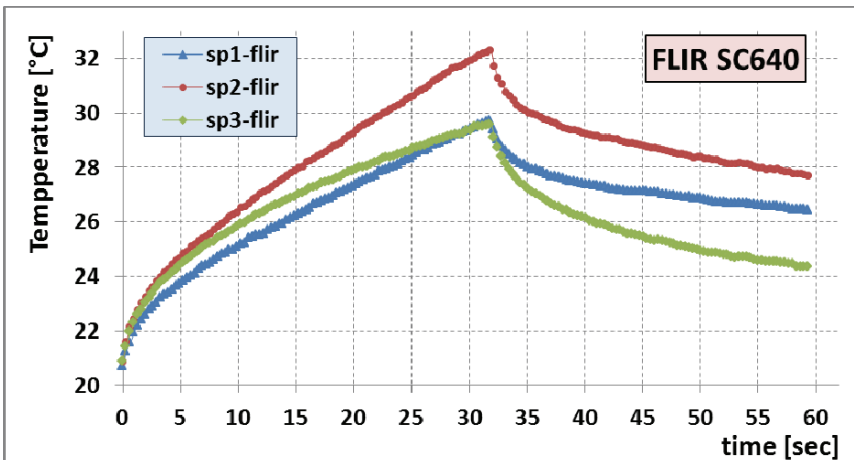
The polycarbonate sample was tested by launching a single square wave with a period of 60 sec, and duty of 50%. For this test it was possible to simultaneously acquire the temperature with two IR cameras positioned one next to the other: the Varioscan 3022 already described in section 2.2, and a FLIR ThermaCAM™ SC 640. This second IR camera is a focal plane array microbolometer which then operates in the long-wave IR spectral range, contrarily to the Varioscan MCT detector which operates in the 3-5 μm mid-wave infrared spectral range. Also another remarkable difference is the thermal resolution with the FLIR camera having a NETD of 30 mK. Figures 8b,c report the time-temperature profiles, and fig. 10 the phase-



(a)



(b)



(c)

Figure 8: Temperature *versus* Time curves from single pixels from a) the GRP panel (one curve for each duty cycle test); b) Polycarbonate panel – data from the

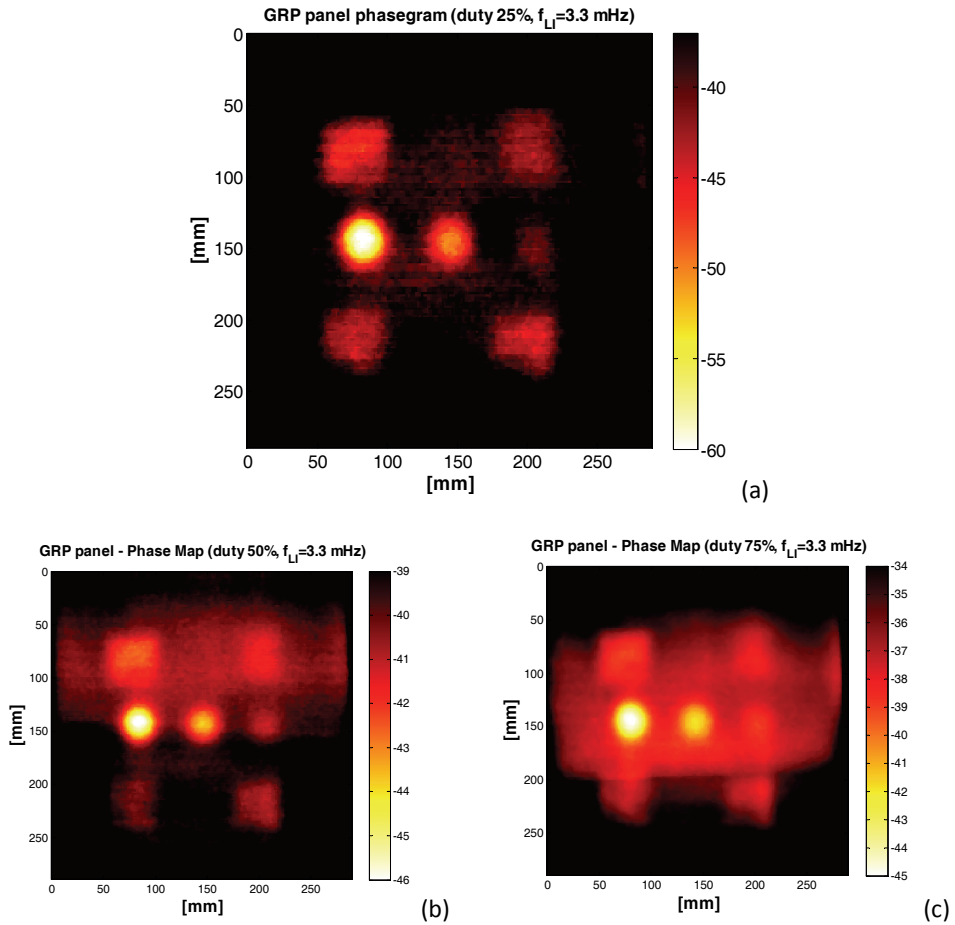


Figure 9: Phase maps from the GRP sample obtained at a Lock-In correlation frequency of 3.3 mHz, and heat deposition modulated with duty cycles of: a) 25%; b) 50%; c) 75%.

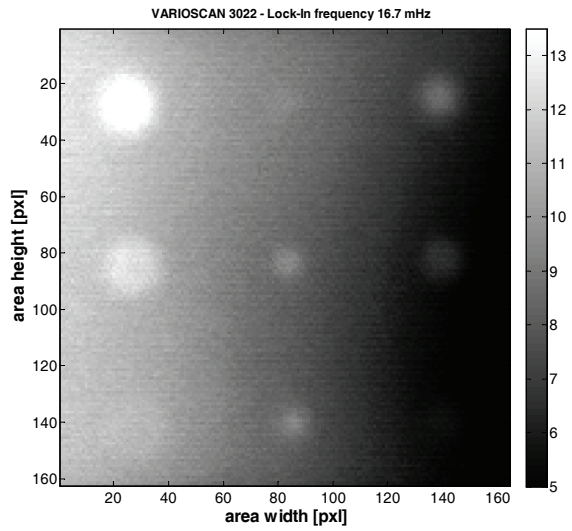
rams obtained by using a lock-in frequency equal to the main carrier frequency, i.e. 16.7 mHz.

A most interesting outcome from this second test is related to the temperature profiles of fig. 8b,c. The three profiles are referred to three pixels whose position is defined in fig. 1d. It is evidenced that temperature from point sp3 is higher than sp1 due to the fact that the lamp was placed laterally on the right, at an angle of about 30°, with respect to the sample. This produced a non-uniform heat deposition with the right hand side of the sample receiving more heat. It is then observed that the FLIR camera does not detect a sudden jump when switching on/off the lamp, while the Varioscan (see both figs. 8a and 8b) does show a sudden temperature change of several degrees which cannot be due to the real temperature change in the panel. The reason of this behavior is that the Varioscan camera was not able to compensate reflection of the hot halogen lamp, mostly coming from the wall behind the sample which showed a saturated temperature when the lamp was on. The FLIR camera did not suffer such problem, probably due to the different spectral range of its detector. Figure 10 shows also that defects are better contrasted in the phasegram obtained from the data measured by the FLIR camera. It is interesting to observe also that the phase on the sound area is more uniform with the FLIR data. Indeed the uniform phase signal from the sound zones, even in presence of a non-uniform heat deposition, is another point in favor of Lock-In Thermography (see e.g. [Ibarra-Castanedo, Benitez, Maldague, Bendada, A. (2007)]), which again is confirmed also by the not-conventional lock-in analysis implemented in this work.

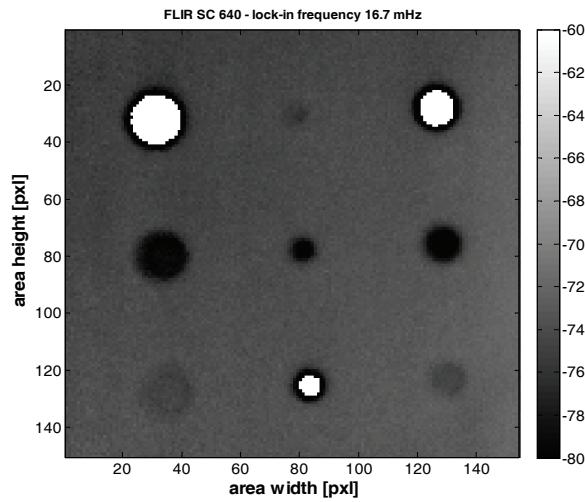
While the better performance of the FLIR camera is clear, it is though remarkable how a much older and cheaper camera such as the Varioscan, not able to get rid of reflection, is still producing phasegrams with well contrasted defects, in both the GRP and Polycarbonate samples. It is believed that this ability of Varioscan to perform well is related with the lock-in algorithm implemented in this work, which is able to selectively filter out specific harmonics buried in the acquired signal, thus operating as a narrow band filter with total freedom of choice over which frequency to use to perform the lock-in correlation.

5 Conclusions

The present work has investigated the feasibility of implementing Transient and Modulated IR Thermography techniques for the NDE of subsurface defects by means of low cost and low performance IR cameras and low power heat sources. The work in particular has successfully investigated thick GRP composite laminates (with delamination defects depths ranging between 3 and 9 mm) and a polycarbonate plate with blind back holes at depths between 1.5 and 6 mm.



(a)



(b)

Figure 10: Phase maps obtained from the Polycarbonate sample at a Lock-In correlation frequency of 16.7 mHz, and data measured with: a) Varioscan 3022; b) FLIR SC 640.

The external heat input is in particular generated by low power halogen lamps, with the possibility to manually control only rather long heat pulse durations.

Regarding the Transient Thermography (TT) approach the cooling transitory was monitored after long heat deposition intervals (longer than 20 seconds) and two definitions of thermal contrast, standard and normalized, were considered for qualitative and quantitative correlation with defects features. The importance of the choice of reference sound areas is highlighted in relation with the occurrence of early thermal contrast during heat deposition, and non-uniformity of heat deposition upon the surface. The influence of a sound area is in particular analyzed in terms of its induced anomalies on the curves of standardized and normalized thermal contrast. A number of features from these curves are discussed which may provide a useful indication about the quantitative interpretation of thermal contrast parameters. The TT approach was able to provide excellent qualitative detection of shallow defects (3 mm depth), good quantitative interpretation for mid-depth defects (6 mm), and only qualitative barely visible detection of deeper defects (9 mm).

Regarding the implemented Modulated Thermography approach, this adopted a customized and off-line lock-in signal treatment which allowed the use of a manually controlled heat modulation. This in particular consisted into a train of square waves with different periods and duty cycles. The off-line lock-in signal post-processing allowed obtaining phase maps which enhanced the qualitative detectability of all defects with respect to the TT approach. Furthermore the implemented lock-in treatment showed to be particularly versatile, in that it can rapidly evaluate different lock-in frequency values, and robust, in that it is able to deal very well with noisy data and with disturbances such as environment reflection, both likely to occur when testing in-situ.

Acknowledgement: The author would like to thank Mr. Federico Riforgiato and Mr. Antonino Licari who have provided a precious help in the collection of experimental data processed in this work and Mr. Giovanni Di Stefano of IMC Service s.r.l. for allowing the use of the FLIR SC 640 infrared camera as described in the paper.

References

- Amenabar, I.; Mendikute, A.; López-Arraiza, L.; Lizaranzu, M.; Aurrekoetxea, J.** (2011): Comparison and analysis of non-destructive testing techniques suitable for delamination inspection in wind turbine blades. *Composites: Part B*, vol. 42, 1298–1305.
- Arndt, R. W.** (2010): Square pulse thermography in frequency domain as adap-

tation of pulsed phase thermography for qualitative and quantitative applications in cultural heritage and civil engineering, *Infrared Physics & Technology*, vol. 53, 246–253.

Avdelidis, N.P.; Almond, D.P.; Dobbinson, A.; Hawtin, B.C.; Ibarra-Castanedo, C.; Maldague, X. (2004): Aircraft composites assessment by means of transient thermal NDT", *Progress in Aerospace Sciences*, vol. 40, no. 3, pp. 143-162.

Balageas D. (2010): Personal thoughts on the occasion of the Xth QIRT Conference. *QIRT 2010*-161.

Benitez, H. D.; Loaiza, H.; Caicedo, E.; Ibarra-Castanedo, C.; Bendada, A. H.; Maldague, X. (2009): Defect characterization in infrared non-destructive testing with learning machines, *NDT&E International*, 42, 630.

Breitenstein, O.; Warta, W.; Langenkamp, M. (2010): *Lock-in Thermography*, Springer, 2nd Ed.

Busse, G.; Wu, D.; Karpen, W. (1992): Thermal Wave imaging with phase sensitive modulated thermography, *J. Appl. Phys.* 71, 3962.

Chatterjee, K.; Tuli, S.; Pickering, S. G.; Almond, D. P. (2011): A comparison of the pulsed, lock-in and frequency modulated thermography non destructive evaluation techniques. *NDT&E International*, vol 44, 655–667.

Choi, M.; Kang, K.; Park, J.; Kim, W.; Kim, K. (2008): Quantitative determination of a subsurface defect of reference specimen by lock-in infrared thermography, *NDT&E International*, vol. 41, 119–124.

Dumoulin, J.; Ibarra-Castanedo, C.; Quiertant, M.; Taillade, F.; Bendada, A.; Maldague, X. (2010): Evaluation of FRP gluing on concrete structures by active infrared thermography. *Qirt 2010*, July 27-30, 2010, Québec (Canada).

Garnier, G; Pastor M. L.; Eyma, F.; Lorrain, B (2011): The detection of aeronautical defects in situ on composite structures using Non Destructive Testing. *Composite Structures*, vol. 93, 1328–1336.

Ghali, V. S.; Mulaveesala, R. (2011): Comparative Data Processing Approaches for Thermal Wave Imaging Techniques for Non-Destructive Testing. *Sens Imaging*, vol. 12, 15–33.

Giorleo, G.; Meola, C. (2002): Comparison between Pulsed and Modulated Thermography in Glass-Epoxy Laminates, *NDT&E International* vol. 35, 287.

Greene, E. (2012): Inspection Technique For Marine Composite Construction and NDE. Ship Structure Committee project SR-1464, Report No. 463.

Ibarra-Castanedo, C. (2005): Quantitative subsurface defect evaluation by Pulsed Phase thermography: Depth Retrieval with the Phase, PhD thesis. Faculté des sciences et de Génie Université Laval Québec.

Ibarra-Castanedo, C.; Benitez, H.; Maldague, X.; Bendada, A. (2007): Review of thermal-contrast-based signal processing techniques for the nondestructive testing and evaluation of materials by infrared thermography, *International Workshop on Imaging Nondestructive Evaluation*, Chennai, India, 25-28 April 2007.

Ibarra-Castanedo, C.; Genest, M.; Avdelidis, N.; Jen, C. H.; Piau, J. M.; Guilbert, S.; Maldague, X. P.; Bendada, A. (2009): Comparative study of active thermography techniques for the nondestructive evaluation of honeycomb structures, *Res Nondestr Eval*, 20, 1–31.

Krapez, J. C.; Balageas, D. (1995): Early detection of thermal contrast in pulsed stimulated infrared thermography, *Proc. QIRT 94*, Paris, 1995, 260-266.

Liu, J.; Wang Y.; Dai J. (2010): Research on thermal wave processing of lock-in thermography based on analyzing image sequences for NDT, *Infrared Physics & Technology*, vol. 53, 348–357.

Maldague, X. (2003): *Theory and Practice of Infrared Technology for Non-Destructive Testing*. Wiley, New York.

Maldague, X.; Marinetti, S. (1996): Pulse Phase Infrared Thermography, *J. Appl. Phys.*, 79 [5], 2694.

Martin, R. E.; Gyekenyesi, A. L.; Shepard, S. M. (2003): Interpreting the Results of Pulsed Thermography Data, *Mater. Eval.*, vol. 61(5), 611-616.

Meola, C.; Carlomagno, G. M. (2004): Recent advances in the use of infrared thermography, *Meas. Sci. Technol.*, vol. 15, 27.

Montanini, R. (2010): Quantitative determination of subsurface defects in a reference specimen made of Plexiglas by means of lock-in and pulse phase infrared thermography. *Infrared Physics & Technology*, vol. 53, 363–371.

Pickering, S. G.; Almond, D. P. (2010): Comparison of the defect detection capabilities of flash thermography and vibration excitation shearography. *Qirt 2010*. July 27-30, 2010, Québec (Canada).

Pitarresi, G.; D'acquisto, L.; Siddiolo, A. M. (2008): Thermoelastic stress analysis by means of an infrared scanner and a two-dimensional fast Fourier transform-based lock-in technique, *J. Strain Analysis* vol. 43, 493.

Pitarresi, G. (2010): Thermal NDE of thick GRP panels by means of a Pulse Modulated Lock-In Thermography technique, *EPJ Web of Conferences* 6, 38014.

Pitarresi, G. (2012): Implementation of a fast and low cost IR-NDT technique by means of a Square Pulse Modulated Lock-In Thermography. 11th International QIRT Conference on Quantitative InfraRed Thermography, n. 343, Naples, 11-14 June 2012.

Polimeno, U.; Almond, D. P. (2009): A compact thermosonic inspection system

for the inspection of composites. Proceedings of International Conference on Composite Materials - ICCM 17, Edinburgh 26-29 July 2009.

Ptaszek, G.; Cawley, P.; Almond, D.; Pickering, S. (2012): Artificial disbonds for calibration of transient thermography inspection of thermal barrier coating systems, *NDT and E International*, vol. 45, no. 1, pp. 71-78.

Shepard, S. M.; Hou, J.; Lhota, J. R.; Golden, J. M. (2007): Automated processing of thermographic derivatives for quality assurance, *Optical Engineering* vol. 46(5), 051008-1.

Sheppard, P. J.; Phillips H. J.; Cooper, I. (2009): The practical use of NDE methods for the assessment of damaged marine composite structures, Proceedings of ICCM 17, Edinburgh (UK) 27-31, July 2009.

Susa, M.; Maldague, X.; Boras, I. (2010): Improved method for absolute thermal contrast evaluation using Source Distribution Image (SDI), *Infrared Physics & Technology* 53, 197–203.

Taillade, E.; Quiertant, M.; Benzarti, K.; Aubagnac, C. (2011): Shearography and pulsed stimulated infrared thermography applied to a nondestructive evaluation of FRP strengthening systems bonded on concrete structures, *Construction and Building Materials*, vol. 25, 568–574.

Wu, D.; Busse, G. (1998): Lock-in thermography for non-destructive evaluation of materials, *Rev. Gén. Therm.*, 37, 693.

